

## **New Ti-6Al-2Nb-2Ta-1Mo alloy as implant biomaterial:**

### ***In vitro* corrosion and *in vivo* osseointegration evaluations**

Lucia Carmen Trincă<sup>1,\*</sup>, Daniel Mareci<sup>2</sup>, Carmen Solcan<sup>3</sup>, Mircea Fântânariu<sup>4</sup>, Liviu Burtan<sup>4</sup>, Luminița Hritcu<sup>4</sup>, Ciprian Chirută<sup>4</sup>, Luis Fernández-Mérida<sup>5</sup>, Raquel Rodríguez-Raposo<sup>5</sup>, Juan J. Santana<sup>6</sup>, Ricardo M. Souto<sup>5,7,\*</sup>

<sup>1</sup> Exact Sciences Department, "Ion Ionescu de la Brad" University of Agricultural Sciences and Veterinary Medicine, Faculty of Horticulture, Str. Aleea M. Sadoveanu, no. 3, 700490, Iasi, Romania.

<sup>2</sup> Department of Chemical Engineering, Technical University "Gheorghe Asachi" of Iasi, Faculty of Chemical Engineering and Environmental Protection, D. Mangeron, Iasi, 700050, Romania.

<sup>3</sup> Preclinics Department, "Ion Ionescu de la Brad" University of Agricultural Sciences and Veterinary Medicine, Faculty of Veterinary Medicine, Str. Aleea M. Sadoveanu, no. 8, 700489, Iasi, Romania.

<sup>4</sup> Clinics Department, "Ion Ionescu de la Brad" University of Agricultural Sciences and Veterinary Medicine, Faculty of Veterinary Medicine, Str. Aleea M. Sadoveanu, no. 8, 700489, Iasi, Romania.

<sup>5</sup> Department of Chemistry, Universidad de La Laguna, Avda. Astrofisico Francisco Sánchez s/n, E-38200 La Laguna (Tenerife, Canary Islands), Spain.

<sup>6</sup> Department of Process Engineering, Universidad de Las Palmas de Gran Canaria, Campus Universitario de Tafira, E-35017 Las Palmas de Gran Canaria, Spain.

<sup>7</sup> Institute of Materials Science and Nanotechnology, Universidad de La Laguna, P.O. Box 456, E-38200 La Laguna (Tenerife, Canary Islands), Spain.

## Abstract

Over the last decade, new titanium alloys are developed in different areas of implantology. The aim of this study was to characterize a new Ti-Al-Nb-Ta-Mo based alloy, with high potential for being used as a biomedical implant. The evaluation of Ti-6Al-2Nb-2Ta-1Mo was performed both *in vitro* (by monitoring its corrosion resistance in Hank's Balanced Salt Solution, HBSS) and *in vivo* (by evaluating the osseointegration following rabbit tibia implantation), by comparison with titanium and Ti-6Al-7Nb alloy. Electrochemical impedance spectroscopy (EIS) data showed high impedance values for all titanium samples after 1 week immersion times in HBSS at 37 °C. According to EIS analysis, the corrosion resistance of the Ti-6Al-2Nb-2Ta-1Mo alloy immersed in HBSS was higher compared to the standard cp-Ti or with the Ti-6Al-7Nb alloy. In addition, a higher degree of osseointegration was achieved by the Ti-6Al-2Nb-2Ta-1Mo alloy, thus probing that a higher resistance to electrochemical corrosion provided enhanced protection to the implant surface against biodegradation, thus positively affecting the qualitative and quantitative evolution of bone tissue repair.

**Keywords:** Ti-Al-Nb-Nb-Ta-Mo biomaterial; *in vitro* corrosion testing; *in vivo* osseointegration evaluation; electrochemical impedance spectroscopy; computed tomography; rabbit animal model.

## 1. Introduction

The search for alternative alloys to conventional precious materials has become a major objective in Materials Science in recent times. In the quest to develop new metal alloys, the evaluation of their corrosion properties is an important request, because corrosion processes are essential phenomena affecting the biocompatibility of an implant alloy. Indeed, the different behaviour of various implant alloys is related to the mechanism responsible for their corrosion resistance. Noble metals present good resistance to corrosion due to the low reactivity induced by their electrochemically stable structure. Base metals such titanium, and titanium-based alloys, exhibit a high affinity for oxygen thus developing passive oxide films on their surface in physiological environments [1,2], which act as protective layers against corrosion [3-7]. Although titanium is a base metal thermodynamically, with a low redox potential in aqueous solutions, passivity is conferred by the very stable and tenaciously adherent passivating oxide film spontaneously formed over the surface [8,9], and it reforms very rapidly if removed or mechanically damaged. The actual composition of the passive film remains controversial, but it is mostly agreed that the film consists of titanium dioxide,  $\text{TiO}_2$ , and it contains anionic vacancies accounting for  $n$  semiconductor characteristics [1,10,11].

Titanium-based materials are very resistant materials to corrosion in human body fluids [12,13], although titanium corrosion products (e.g. in the form of submicrometer particles) are often observed in tissues adjacent to implant prosthesis [14]. These corrosion products have been attributed to the formation of the oxide layer [15], to transient breakdown and reforming events of this film [16], and to metal debris [17]. In addition, acidification is considered harmful for the stability of the passive regime [18]. Though titanium appears to be tolerated in the body in minute amounts, the long term effect of its accumulation and the fact that it is not excreted remains of biological concern. When the prostheses are placed in the human body, the passive films undergo further transformations, namely thickening of the passivating film and stoichiometric changes, as well as metal dissolution [15,19,20]. It must be taken into account that both passivation and metal dissolution are processes of an electrochemical origin [21].

The standard Ti-6Al-4V implant alloy was the first titanium alloy biomaterial employed in implantable components and devices (particularly for orthopaedic and osteosynthesis applications), and it is still widely used in restorative medicine. Yet growing concerns for its usage arise from evidences that even small amounts of vanadium, when released in the human

body, may induce cytotoxic effects [22]. Due to the potential toxicity of alloying elements like V and Al in the standard Ti-6Al-4V alloy, new titanium-based alloy biomaterials are developed that contain non-toxic elements such as Nb, Zr, Ta, and Mo. In this context, the Ti-6Al-7Nb alloy was proposed as an alternative to the Ti-6Al-4V alloy because it exhibited better corrosion and wear resistances [22], and it has become commercially available as ASTM F-1295. Ti-6Al-7Nb is a high strength ( $\alpha + \beta$ ) Ti-alloy, with Al stabilizing the hexagonal  $\alpha$ -phase and Nb stabilizing the  $\beta$ -body-centered phase [23]. Ti-6Al-7Nb showed a high biocompatibility to the human body, and its oxides did not induce adverse tissue tolerance reactions. When implanted in a bone model, Ti6Al7Nb was well integrated into fibrous tissue and no inflammatory reaction was seen. Even one month after implantation, Ti-6Al-7Nb showed bone formation at the edge of the implant [24]. Furthermore, hydroxyapatite-coated Ti-6Al-7Nb implant showed enhancement of osteoconductive capacity, probing that chemistry and surface topography are key factors influencing osseointegration [25,26]. Unfortunately, Ti6Al4V and Ti6Al7Nb exhibit a relatively high Young modulus compared to the value of cortical bone (100-110 and 15-25 GPa, respectively [27]), which may result in early bone failure [28].

Further biocompatibility enhancement and lower modulus can be achieved by synthesizing new titanium alloys such as Ti-6Al-2Nb-1Ta-1Mo. Tribological investigations have shown that Ti-6Al-2Nb-1Ta-1Mo alloy is a near alpha wrought alloy. Near-alpha alloys contain small amounts of ductile beta-phase. The Ti-6Al-2Nb-1Ta-1Mo alloy is known to possess high toughness, medium strength, weldability, and resistance to seawater corrosion. It is however not heat-treatable. Ti-6Al-2Nb-1Ta-1Mo alloy can be hot or cold formed [29]. Hot working enhances the overall ductility of the material. Cold working features of this material is same as that of a moderately tempered austenitic stainless steel. Post-work annealing is recommended to re-attain favorable performance properties [30]. Since the corrosion resistance of Ti-6Al-2Nb-1Ta-1Mo alloy is comparable to commercial pure titanium and Ti-6Al-4V, this vanadium-free alloy is expected to remain stable in the living body as well [31].

Before being used in implantology, any new biomaterial must undergo a complex sequence of characterizations, including both *in vitro* and *in vivo* evaluations [32]. Amongst the electrochemical techniques used for *in vitro* corrosion studies, the alternating current impedance method has the advantages of being an optimally, non-destructive technique [33-37] that efficiently monitors the specific aspects related to the electrochemical performance of implant

materials. Since these new biomaterials may remain inside the patient's body over long periods of time, sometimes spanning their entire life, the potential risk of corrosion and the eventual detrimental effects of their byproducts are significant issues that require complex clinical interdisciplinary (physico-biochemical, histological and radiological) investigations.

The purpose of this study was to evaluate the *in vitro* corrosion and *in vivo* osseointegration of a newly-synthesized Ti-6Al-2Nb-2Ta-1Mo alloy with potential biomaterial applicability. For the sake of comparison, similar tests were also performed on pure titanium (cp-Ti) and the Ti-6Al-7Nb alloy. Potentiodynamic polarization and electrochemical impedance spectroscopy tests were performed in Hank's balanced physiological solution, whereas animal model testing was conducted by implanting cylindrical rods of these materials in the tibial crest of rabbits, whereas monitoring biochemical, histological and computed tomography data at different elapsed times after surgery.

## **2. Experimental**

### **2.1. Materials**

The titanium-based materials used in this work were commercial titanium (cp-Ti, 99.99 wt.% Ti), Ti-6Al-7Nb (5.8 wt.% Al, 7.2 wt.% Nb, Ti in balance), and the new Ti-6Al-2Nb-2Ta-1Mo alloy. Cp-Ti and Ti-6Al-7Nb alloy were purchased from the Rare and Non-Ferrous Metals Institute (Bucharest, Romania) with rod-like shape. In brief, the Ti-6Al-2Nb-2Ta-1Mo alloy was synthesized by the cold crucible levitation melting (CCLM) technique in an induction furnace (Fives Celes, Lautenbach, France) under a pure Ar atmosphere. Further details of the method are described in ref. [38]. The melting procedure was repeated three times to obtain the chemically homogenized alloy. The final chemical composition was 5.8 wt.%Al, 2.2 wt.% Nb, 2.3 wt.% Ta, 1.3 wt.% Mo, and Ti in balance.

### **2.2. Surface and material characterization**

The structure of the Ti-6Al-2Nb-2Ta-1Mo alloy was characterized by X-ray diffraction (XRD) at ambient temperature using a Philips PW 1830/00 (Eindhoven, The Netherlands) diffractometer using  $\text{CuK}\alpha_1$  radiation (e.g., 1.5406 Å wavelength). The surface microstructure of the alloy was characterized by optical microscopy using a Leica DM RM system (Wetzlar,

Germany). Prior to optical imaging, the samples were first mechanically abraded using a sequence of silicon carbide abrasive papers followed by a final polishing step with a colloidal silica suspension (particle size: 50 nm). Samples were observed under polarized light to enhance the phase contrast. The microstructure was revealed by etching in 10% HF + 5% HNO<sub>3</sub> solutions for 3-5 s at room temperature.

The surface topography of the specimens after electrochemical testing in HBSS was observed by scanning electron microscopy (SEM). SEM observations were made using a Quanta 200 (FEI, Hillsboro, OR, USA) operated at an accelerating voltage of 30 keV.

### **2.3. *In vitro* corrosion tests**

Hank's Balanced Salt Solution (HBSS) was selected as simulated physiological environment for the *in vitro* corrosion tests [39]. Prior to electrochemical testing, the samples were mechanically abraded using a sequence of SiC papers up to 4000 grit, subsequently polished using 1 mm alumina suspension, and finally cleaned in ethyl alcohol. The titanium alloys were introduced as working electrodes in a glass corrosion flow cell kit (C145/170, Radiometer, France) [40]. A saturated calomel electrode (SCE) was used as reference electrode and a platinum wire as auxiliary electrode. The electrochemical cell was filled with naturally-aerated HBSS. Electrochemical measurements were carried out at 37 °C, and they were initiated after the samples were immersed for 1 week in HBSS at their open circuit potential.

The electrochemical techniques used for corrosion characterization were open circuit potential measurements, potentiodynamic polarization curves, and electrochemical impedance spectroscopy (EIS). These measurements were performed using a PARSTAT 4000 potentiostat controlled by a personal computer with dedicate software (*Power Corr*, Princeton Applied Research, Princeton, NJ, USA). Electrochemical impedance spectra were measured over a frequency range extending from 100 kHz to 1 mHz using a 10 mV amplitude for the sinusoidal AC voltage signal. The EIS tests were recorded at the open circuit potential developed by the samples after one-week immersion in the HBSS. EIS data were recorded to evaluate the characteristics of passive films formed on the surface of the alloys under investigation. Analysis of the spectra was performed in terms of equivalent circuit (EC) fitting using *ZSimpWin* software [41]. Subsequently, linear polarization plots were recorded at a 1 mV/s scan rate from -1.0 V<sub>SCE</sub> up to +1.0 V<sub>SCE</sub>.

## **2.4. *In vivo osseointegration evaluation***

Implantation was performed by surgical operation on the left tibial crest of the anesthetized animal as shown in Figure 1. The implants (cylindrical shape, 3 mm diameter, 9 mm length) were implanted in 3 months old male rabbits (approximately 1.8 kg weight). During the experiment, the animals were housed with free access to food and water according to standard ISO10993-2:2006 on animal welfare [42]. The experimental model was conducted for a month. The body's response to implant animal was monitored by clinical observations, by radiological investigations and biochemical analyzes on blood samples collected every 7 days. Also, the response of the animal body to the implant was monitored by histopathological investigations on bone samples, harvested at the end of the experimental period.

### **2.4.1. *Biochemical analysis***

Blood samples were collected by cardiac puncture under anesthetic condition in the 28<sup>th</sup> day after the implantation procedure. Analyses were performed at the Clinical and Biochemical Laboratory (Faculty of Veterinary Medicine, Iasi). Serum was separated by centrifugation, and inorganic phosphate ( $\text{PO}_4^{3-}$ ), ionic calcium ( $\text{Ca}^{2+}$ ), alkaline phosphatase (ALP), and total proteins (TP) were spectrophotometrically [43] determined by using BS-130 Biochem Automatic Analyzer and Liquick Cor-PZ kit tests (Cormay, Łomianki, Poland).

### **2.4.2. *Histologic analysis***

The callus along with normal bone was collected from the fracture site. The samples were cut into small pieces and stored in 10 vol.% formalin solution for three days, demineralized with 10 vol.% trichloroacetic acid, dehydrated in ascending grades of alcohol, and embedded in paraffin. Five to six micrometer thick sections of the area close to the defect site were cut and prepared for staining with hematoxylin and eosin (H&E) staining method for histological studies [44]. The stained sections were examined under light microscope by using 100 - 1000× magnifications.

### **2.4.3. *CT analyses***

A high-resolution CT system (X-ray CT, Siemens Somatom, Balance, Erlangen, Germany) was employed to evaluate the microstructure of each rabbits's left back member, with a scanning resolution of 20  $\mu\text{m/slice}$ . After scanning, 3-D images were reconstructed based on the acquired 2-D image sequences, by using the image software *Synego Viewer*, Version 2.21. The trabecular bone parameters, including bone volume per tissue volume (BV/TV), trabecular thickness (Tb.Th) and trabecular separation (Tb.Sp) were quantified by using *ImageJ* and *BoneJ* software [45]. Region of interest was defined by adding 1 mm both in width and height to the implant contour of oval shape.

#### *2.4.4. Statistical analysis*

Statistical analyses were performed *IBM SPSS Statistics* (IBM Corp. Released 2012 IBM SPSS Statistics for Windows, Version 21.0; IBM Corp, Armonk, NY, USA) [46]. All data were examined for normal distribution using the Shapiro-Wilk test. Analyses showed that each specific parameter for the *in vivo* data obeyed normal heterogeneous distribution. For all *in vivo* biochemical results, the differences of each parameter between the experimental group and Control group were examined using Student t-test. For CT analyses, one-way analysis of variance (ANOVA) was employed for evaluating the differences among the groups ( $p < 0.05$  was considered statistically significant difference).

### **3. Results and Discussion**

#### ***3.1. Material characterization***

A typical XRD pattern from the Ti-6Al-2Nb-2Ta-1Mo alloy is shown in Figure 2, evidencing the material to be a body-centered cubic structure. All the peaks in the diffractograms were unambiguously indexed according to this crystallographic structure, and the corresponding diffracted planes are labeled in the plot. On the other hand, the micrograph depicted in Figure 3 shows the microstructure of the Ti-6Al-2Nb-2Ta-1Mo alloy after chemical etching of the surface.  $\beta$  equiaxial grains are observed, in good agreement with the XRD observations.

#### ***3.2. In vitro corrosion characterization***



Electrochemical techniques were employed to characterize the corrosion resistance of the Ti-6Al-2Nb-2Ta-1Mo alloy *in vitro*, whereas scanning electron microscopy (SEM) was employed to determine the surface morphology of the surface layers responsible for their passivity after completing the electrochemical tests. The measurements were conducted during immersion of the samples in Hank's Balanced Salt Solution (HBSS) at 37 °C. Potentiodynamic polarization and electrochemical impedance spectroscopy measurements were performed after 1-week free immersion in the simulated physiological solution. For the sake of comparison, the measurements were made in triplicate, and samples of pure titanium (cp-Ti) and Ti-6Al-7Nb were tested in the same conditions.

### 3.2.1. Electrochemical impedance spectroscopy analysis

EIS measurements were performed under open circuit potential conditions in aerated HBSS at 37 °C, and they were initiated after 1 week immersion. Typical impedance spectra of cp-Ti, Ti-6Al-7Nb and Ti-6Al-2Nb-2Ta-1Mo are presented as Nyquist, Bode-phase and Bode-magnitude plots in Figure 4. It is readily observed that these materials present similar impedance spectra displaying two maxima in the Bode-phase graphs. Thus, they can be separated into two distinct frequency ranges: one time constant in the high-frequency region that arises from the uncompensated ohmic resistance due to the simulated physiological solution and the impedance behaviour resulting from the penetration of the electrolyte through a porous film, and a low-frequency region originating from the processes occurring at the substrate/solution interphase. This fact agrees with the observation that passive films formed on pure titanium and titanium alloys generally consist of two layers [3,47], a thin compact oxide in direct contact with the unoxidized metal in the matrix, and a thicker and more porous outer layer that contacts the environment [48,49].

Analysis of the impedance spectra was performed by fitting an equivalent circuit (EC) to the experimental data, where the circuit elements represent electrochemical characteristics of the material and its oxide film. The impedance diagrams depicted in Figure 4 show both the experimental data obtained from the Ti-based materials as discrete points, whereas the lines correspond to the fitted results for the EC given in Figure 5. This equivalent circuit has been employed to describe the impedance behavior of various Ti-based materials exposed to physiological solutions [50-57]. The barrier characteristics of the oxide film towards electrolyte

penetration that dominates the impedance response in the low-frequency range are described by the time constant  $R_1 Q_1$ ), whereas the charge transfer process in the surface of the alloys at higher frequencies is represented by  $R_2$  and  $Q_2$ .

Instead of pure capacitors, constant phase elements (CPE) were introduced in the fitting procedure to obtain good agreement between the simulated and experimental data. The impedance of a CPE is given by [58]:

$$Z_{\text{CPE}} = \frac{1}{Q(j\omega)^n} \quad (1)$$

where  $Q$  is the combination of properties related to both the surface and electroactive species that is independent of frequency;  $n$  is related to the slope of the Bode-amplitude plot;  $\omega$  is the angular frequency; and  $j$  is imaginary number ( $j^2 = -1$ ).  $Q$  is an adjustable parameter used in the fitting routine, and when the value of  $n$  is equal to 1, the CPE acts as a pure capacitor. The value of the fit exponent  $n$  corresponds to the extent of dispersion and is attributed to surface inhomogeneity. The quality of fitting to the equivalent circuit was judged from the optimum combination of the chi-square ( $\chi^2$ ) value and the error distribution vs. frequency that compared experimental to simulated data.

Table 1 contains the values of fitted parameters to the EC for the impedance spectra of Figure 4. The same values for  $R_{\text{sol}}$  ( $64 \pm 5 \Omega \text{ cm}^2$ ) were determined for all the Ti-based materials and they are not included in Table 1. The main observation is that high values of  $R_1$  (in the order of  $\text{M}\Omega \text{ cm}^2$ ) were obtained for the three materials during exposure to aerated HBSS at their open circuit potential values, a feature that confirms the validity of the EC that implies the formation of a duplex oxide film containing a compact inner layer on the samples. Beyond this similarity, the enhanced corrosion resistance of the new Ti-6Al-2Nb-2Ta-1Mo alloy compared to cp-Ti and even to Ti-6Al-7Nb is demonstrated by this material delivering the greatest  $R_1$  value of the three. Even in the case of the outer layer, despite its general non-sealing character that facilitates the eventual contact of the electrolyte to the base metal through pores, attains the greatest value of  $R_2$  among the three materials. Therefore, EIS data support that a highly resistant passive layer is formed spontaneously on the Ti-6Al-2Nb-2Ta-1Mo alloy upon exposure to a simulated physiological environment, effectively providing a lower susceptibility for corrosion to this alloy compared to cp-Ti and Ti-6Al-7Nb, which have been accepted as suitable biomaterials for implantation in the human body.

### 3.2.2. Potentiodynamic polarization plots

The passivity condition of the samples immersed in aerated HBSS at 37 °C was further investigated by recording potentiodynamic polarization plots at 1 mV/s scan rate, and they are depicted in Figure 6. The potential excursion in the positive direction reached +1.0 V<sub>SCE</sub>, a value significantly higher than any polarization ever measured in the human body [59].

The shape of the anodic branches confirmed the onset of passivity for the materials in HBSS at 37°C. Tafel analysis of both the anodic and cathodic branches of the polarization plots delivered values for ZCP and corrosion current densities ( $j_{cor}$ ), as well as the corresponding Tafel slope values (i.e.,  $\beta_a$  and  $\beta_c$ , respectively). Table 2 shows the average values determined for these parameters. The higher values of  $\beta_a$  compared to those for  $\beta_c$  in all cases evidenced an anodic control in the corrosion process. The control implies the existence of a passive layer on the material surface. The oxide layer on the samples gives rise to a typical passive state with a low corrosion current density appearing as current plateaus in all the plots at potentials more positive than their corresponding corrosion potential values (ZCP). Interestingly, the lowest current density required to sustain the passive state was exhibited by the Ti-6Al-2Nb-2Ta-1Mo alloy.

### 3.2.3. Scanning electron microscopy

After completing the electrochemical tests described in the previous sections, the samples were removed from the HBSS solution while polarized at the positive potential limit, namely +1.0 V<sub>SCE</sub>. That is, while they were subjected at anodic polarization. In this way, the final state of the exposed surfaces resulting from *in vitro* exposure could be explored for morphological comparison. The micrographs displayed in Figure 7 show surface roughening related to the development of the passive oxide film, and the total absence of defects related to the onset of localized corrosion processes. The preferential direction of surface preparation during the grounding stage prior to electrochemical exposure were still clearly observable in the micrographs A and B, and less noticeable for the micrograph C. This supports the growth of a thicker oxide film on the Ti-6Al-2Nb-2Ta-1Mo alloy.

## 3.3. *In vivo* osteintegration evaluation

Animal testing was conducted by implanting cylindrical rods of the three materials under investigation in the tibial crest of rabbits, whereas monitoring biochemical, histological and computed tomography data at different elapsed times after surgery.

### *3.3.1. Dynamics of biochemical markers in the implanted animal*

The dynamics of body reaction during the clinical tests was monitored on a weekly basis by collecting blood samples and separating the serum. Inorganic phosphate ( $\text{PO}_4^{3-}$ ), ionic calcium ( $\text{Ca}^{2+}$ ), alkaline phosphatase (ALP), and total proteins (TP) were monitored as key biochemical markers and the obtained values are plotted in Figure 8. Insignificant variations ( $p > 0.05$ ) for any combination of experimental groups were found, thus sustaining a similar biochemical functionality of all tested implants.

Moreover, the parity variation of these biochemical parameters can be correlated with local processes involved in the bone fracture repair. Therefore, the decreased values of ionic calcemia, inorganic phosphatemia, as well as alkaline phosphatase activity in the first 14 days after the implantation surgery appear as a much-delayed response of the metabolic disturbance caused by the stress of surgery trauma [60,61]. Next, between 14-21 days, the increased calcemia and phosphataemia are positively correlated with the activation of alkaline phosphatase, as a normal stage of the bone repair process [43,44]. And the hypocalcemia and hypophosphatemia recorded between 21 and 28 days appear as the first clinical signs of ionic calcium and inorganic phosphates mobilization in the extracellular matrix due to the transformation of fibrocartilaginous callus into primary bone callus [62,63]. Therefore, the stable trend activity of the alkaline phosphatase, that occurs between 21-28 days after the implantation surgery, is induced by the transformation of the osteoblasts into osteoclasts that will be entrapped by the mineralized extracellular matrix.

### *3.3.2. Hystological characterization*

According to Figure 9, bone tracts exhibited osteocytes in the bone gaps as well as mature and immature fundamental substance differentiated by the alternating shades of red to pink colour. The bony osteons were the smallest for the cp-Ti group, being conformed by 3-5 bone lamellae.

In the proximity of the newly bone tissue there are proliferated osteoprogenitor cells that also may be found in bone areoles. Attached to the bone tracts, osteoblasts arranged on a single row were observed for cp-Ti and Ti-6Al-7Nb groups, as well as on two or three rows for the Ti-6Al-2Nb-2Ta-1Mo group. Similarly, in the case of a close-related alloy, *in vitro* cytocompatibility tests showed good colony formation [64], while the current *in vivo* study reported the absence of inflammatory reactions and newly formed bone around the Ti-6Al-2Nb-2Ta-1Mo alloy that was implanted in bone marrow.

Stimulation of osteogenesis in the case of Ti-6Al-2Nb-2Ta-1Mo by comparison with Ti-6Al-7Nb was determined by the presence of Ta and Mo alloy [1,65], as Ta and Mo exhibits excellent chemical stability and good compatibility similar to that of Ti. Recently, Wang et al. [66] described more stable and continuous osteogenic activity in the case of Ta implanted graft material for bone reconstruction situations, whereas Xu et al. reported that the volume fraction of  $\beta$  phase, porosities and pore sizes increases while the elastic modulus and bending strength decrease with the alloy's increasing Mo content [67]. Moreover, the excellent corrosion resistance was related to the oxidation film of TiO<sub>2</sub>, MoO<sub>2</sub> and MoO<sub>3</sub> naturally formed on the surface. Cell viabilities higher than 94%, indicated favorable cytocompatibility, while the spread, proliferation and differentiation of osteoblast-like cells were activated by the presence of the alloy.

### 3.3.3. Computed tomography evaluation

Computed tomography investigation focused on evaluating the newly formed bone tissue deposited on the surface of the implant materials. The 2D- and 3D-reconstructed images of the implant and the newly formed bone shown in Figure 10 evidence that, among the three experimental groups, the surface of the Ti-6Al-2Nb-2Ta-1Mo implant was covered in greater proportion by a thick layer of newly formed bone.

The bone microstructure was evaluated on the basis of the average quantitative parameters contained in Table 3, namely the bone volume/total volume ratio (BV/TV), the trabecular thickness (Tb.Th), and the trabecular space (Tb.Sp) [68]. The group with the Ti-6Al-2Nb-2Ta-1Mo implant exhibited the highest value for the bone volume/total volume ratio, a fact indicating a more intensive osteogenesis process occurring in this system. In addition, the values

of the trabecular thickness and the trabecular space of the newly-formed bone tissue revealed an extended osteointegration process for the Ti-6Al-2Nb-2Ta-1Mo implant (although statistically insignificant with  $p > 0.05$ ), in good agreement with the conclusions of the biochemical and histological characterizations.

#### **4. Conclusions**

*In vitro* electrochemical tests for cp-Ti, Ti-6Al-7Nb and Ti-6Al-2Nb-2Ta-1Mo alloys performed in Hank's balanced salt solution at 37 °C evidenced the onset of passivity for the three materials.

Electrochemical tests recording the electrochemical impedance spectra and the potentiodynamic polarization curves demonstrated the superior corrosion resistance of the Ti-6Al-2Nb-2Ta-1Mo alloys, leading to larger impedance values for the spontaneously formed passive oxide layer on Ti-6Al-2Nb-2Ta-1Mo alloy compared to Ti-6Al-7Nb and cp-Ti samples in the same environment, in combination with smaller passivation current densities ( $j_{cor}$ ). No signs of localized corrosion processes could be observed from the retrieved samples despite polarization up to +1.0 V<sub>SCE</sub>, more anodic than any potential value ever recorded in the human body.

The present *in vivo* investigation spotlighted the ability of titanium alloys containing Al and Nb to promote higher osteogenesis during the first month after implantation than pure titanium taken as control group (cp-Ti). Among them, the highest osteointegration was achieved by the Ti-6Al-2Nb-2Ta-1Mo alloy, thus probing that materials presenting higher resistance to electrochemical corrosion can exhibit greater protection of the implant surface against biodegradation, thus favorably influencing the qualitative and quantitative evolution of bone tissue repair.

#### **Acknowledgements**

Thanks are due to Prof. T. Gloriant (INSA Rennes) for kindly providing the Ti-6Al-2Nb-2Ta-1Mo alloy used in this work. This work was supported partially by the Romanian National Authority for Scientific Research (CNCS-UEFISCDI, project No. PN-II-

IDPCE-2011-3-0218), and by the Spanish Ministry of Economy and Competitiveness (MINECO, Madrid, Spain) and the European Regional Development Fund (project No. CTQ2016-80522-P).

## References

- [1] M. Geetha, A.K. Singh, R. Asokamani, A.K. Gogia, Ti based biomaterials, the ultimate choice for orthopedic implants – A review, *Progress in Materials Science* 54 (2009) 397-425.
- [2] M. Niinomi, M. Nakai, J. Hieda, Development of new metallic alloys for biomedical applications, *Acta Biomaterialia* 8 (2012) 3888-3903.
- [3] J. Pan, D. Thierry, C. Leygraf, Electrochemical impedance spectroscopy study of the passive oxide film on titanium for implant application, *Electrochimica Acta* 41 (1996) 1143-1153.
- [4] D. Mareci, R. Chelariu, D. Sutiman, D.M Gordin, T. Gloriant, Evaluating electrochemical behaviour of recrystallized titanium alloys in Ringer's solution, *Materials and Corrosion* 62 (2011) 1117-1123.
- [5] M. Dilea, A. Mazare, D. Ionita, I. Demetrescu, Comparison between corrosion behavior of implant alloys Ti6Al7Nb and Ti6Al4Zr in artificial saliva, *Materials and Corrosion* 64 (2013) 493-499.
- [6] J.M. Calderon Moreno, C. Vasilescu, S.I. Drob, E. I. Neacsu, M. Popa, Evaluation of the microstructural, mechanical and anti-corrosive properties of a new ternary Ti–15Zr–5Nb alloy in simulated oral environment, *Materials and Corrosion* 65 (2014) 703-714.
- [7] A.C. Bărbîntă, D. Mareci, R. Chelariu, G. Bolat, C. Munteanu, K. Cho, M. Niinomi, The estimation of corrosion behavior of new TiNbTaZr alloys for biomedical applications, *Materials and Corrosion* 65 (2014) 1017-1023.
- [8] C. Johansson, J. Lausmaa, M. Ask, H.-A. Hansson, T. Albrektsson, Ultrastructural differences of the interface zone between bone and Ti 6Al 4V or commercially pure titanium, *Journal of Biomedical Engineering* 11 (1989) 3-8.
- [9] J. Lausmaa, B. Kasemo, H. Mattson, H. Odelius, Multi-technique surface characterization of oxide films on electropolished and anodically oxidized titanium, *Applied Surface Science* 45 (1990) 189-200.

- [10] M. Niinomi, Mechanical biocompatibilities of titanium alloys for biomedical applications, *Journal of the Mechanical Behaviour of Biomedical Materials* 1 (2008) 30-42.
- [11] W.F. Ho, T.Y. Chiang, S.C. Wu, H.C. Hsu, Mechanical properties and deformation behavior of cast binary Ti-Cr alloys, *Journal of Alloys and Compounds* 468 (2009) 533-538.
- [12] E.W. Collings, Physical metallurgy of titanium alloys, in: R. Boyer, G. Welsch, E.W. Collings (Eds.), *Materials Properties Handbook: Titanium Alloys*, ASM, International, Materials Park, OH, 1994, p. 10.
- [13] S.B. Gabriel, L.H. de Almeida, C.A. Nunes, J. Dille, G.A. Soares, Maximisation of the ration of microhardness to the Young's modulus of Ti-12Mo-13Nb alloy through microstructure changes, *Materials Science and Engineering C* 33 (2013) 3319-3324.
- [14] O. Addison, A.J. Davenport, R.J. Newport, S. Kalra, J.W.F. Mosselmans, D. Proops, R.A. Martin, Do "passive" medical titanium surfaces deteriorate in service in the absence of wear?, *Journal of the Royal Society Interface* 9 (2012) 3161-3164.
- [15] K.E. Healy, P. Ducheyne, The mechanisms of passive dissolution of titanium in a model physiological environment, *Journal of Biomedical Materials Research* 26 (1992) 319-338.
- [16] G.T. Burstein, R.M. Souto, Observations of localised instability of passive titanium in chloride solution, *Electrochimica Acta* 40 (1995) 1881-1888.
- [17] L. Mohan, C. Anandan, Wear and corrosion behavior of oxygen implanted biomedical titanium alloy Ti-13Nb-13Zr, *Applied Surface Science* 282 (2013) 281-290.
- [18] P. Ducheyne, G. Willems, M. Martens, J. Helsen, In vivo metal-ion release from porous titanium-fiber material, *Journal of Biomedical Materials Research* 18 (1984) 293-308.
- [19] J.-E. Sundgren, P. Bodö, I. Lundström, Auger electron spectroscopic studies of the interface between human tissue and implants of titanium and stainless steel, *Journal of Colloid and Interface Science* 110 (1986) 9-20.
- [20] K.E. Healy, P. Ducheyne, Oxidation kinetics of titanium thin films in model physiologic environments, *Journal of Colloid and Interface Science* 150 (1992) 404-417.
- [21] G.T. Burstein, C. Liu, R.M. Souto, S.P. Vines, Origins of pitting corrosion, *Corrosion Engineering Science and Technology* 39 (2004) 25-30.
- [22] M.A. Khan, R.L. Williams, D.F. Williams, In-vitro corrosion and wear of titanium alloys in the biological environment, *Biomaterials* 17 (1996) 2117-2126.



- [23] M. Fellah, M. Labaiz, O. Assala, L. Dekhil, A. Taleb, H. Rezag, A. Iost, Tribological behavior of Ti-6Al-4V and Ti-6Al-7Nb alloys for total hip prosthesis, *Advances in Tribology* (2014), Article ID 451387, 13 pages. doi:10.1155/2014/451387.
- [24] H. Rotaru, G. Armencea, D. Spirchez, C. Berce, T. Marcu, D. Leordean, S.G. Kim, S.W. Lee, C. Dinu, G. Băciuț, M. Băciuț, In vivo behavior of surface modified Ti6Al7Nb alloys used in selective laser melting for custom-made implants. A preliminary study, *Romanian Journal of Morphology and Embryology* 54 (2013) 791-796.
- [25] D. Martini, M. Fini, M. Franchi, V.D. Pasquale, B. Bacchelli, M. Gamberini, A. Tinti, P. Taddei, G. Giavaresi, V. Ottani, M. Raspanti, S. Guizzardi, A. Ruggeri, Detachment of titanium and fluorohydroxyapatite particles in unloaded endosseous implants, *Biomaterials* 24 (2003) 1309–1316.
- [26] A.L. Rosa, M.M. Beloti, Effect of cpTi surface roughness on human bone marrow cell attachment, proliferation, and differentiation, *Brazilian Dental Journal* 14 (2003) 16–21.
- [27] A. Schuh, J. Bigoney, W. Hönle, G. Zeiler, U. Holzwarth, R. Forst, Second generation (low modulus) titanium alloys in total hip arthroplasty, *Materials Science & Engineering Technology* 38 (2007) 1003-1007.
- [28] Y. Song, D.S. Xu, R. Yang, D. Li, W.T. Wu, Z.X. Guo, Theoretical study of the effects of alloying elements on the strength and modulus of  $\beta$ -type bio-titanium alloys, *Materials Science and Engineering A* 260 (1999) 269–274.
- [29] A. Gutiérrez, C. Munuera, M.F. López, J.A. Jiménez, C. Morant, T. Matzelle, N. Kruse, C. Ocal, Surface microstructure of the oxide protective layers grown on vanadium-free Ti alloys for use in biomedical applications, *Surface Science* 600 (2006) 3780-3784.
- [30] K. Maehara, K. Doi, T. Matsushita, Y. Sasaki, Application of vanadium-free titanium alloys to artificial hip joints, *Materials Transactions* 43 (2002) 2936-2942.
- [31] T. Hanawa, Metal ion release from metal implants, *Materials Science and Engineering C* 24(2004) 745-752.
- [32] J. Ureña, S. Tsipas, A. Jiménez-Morales, E. Gordo, R. Detsch, A.R. Boccaccini, In-vitro study of the bioactivity and cytotoxicity response of Ti surfaces modified by Nb and Mo diffusion treatments, *Surface & Coatings Technology* 335 (2018) 148-58.

- [33] A. Hodgson, Y. Mueller, D. Forster, S. Virtanen, Electrochemical characterization of passive films on Ti alloys under simulated biological conditions, *Electrochimica Acta* 41 (2002) 1913-1923.
- [34] M. Metikoš-Huković, E. Tkalčec, A. Kwokal, J. Piljac, An in vitro study of Ti and Ti-alloys coated with sol-gel derived hydroxyapatite coatings, *Surface and Coatings Technology* 165 (2005) 40-50.
- [35] G. Ciurescu, J. Izquierdo, J.J. Santana, D. Mareci, D. Sutiman, S. González, R.M. Souto, Characterization of the localized surface chemical activity of Ti-Mo and Ti-Ta alloys for biomedical applications using scanning electrochemical microscopy, *International Journal of Electrochemical Science* 7 (2012) 7404-7424.
- [36] G. Bolat, J. Izquierdo, J.J. Santana, D. Mareci, R.M. Souto, Electrochemical characterization of ZrTi alloys for biomedical applications, *Electrochimica Acta* 88 (2013) 447-456.
- [37] G. Bolat, D. Mareci, A. Cailean, J.J. Santana, R.M. Souto, Effect of acidic fluoride solution on the corrosion resistance of ZrTi alloys for dental implant application, *Corrosion Science* 87 (2014) 334-343.
- [38] T. Gloriant, G. Texier, F. Sun, I. Thibon, F. Prima, J.L. Soubeyroux, Characterization of nanophase precipitation in a metastable  $\beta$  titanium-based alloy by electrical resistivity, dilatometry and neutron diffraction, *Scripta Materialia* 58 (2008) 271-274.
- [39] D. Mareci, R. Chelariu, G. Ciurescu, D. Sutiman, T. Gloriant, Electrochemical aspects of Ti-Ta alloys in HBSS, *Materials and Corrosion* 61 (2010) 768-774.
- [40] D. Mareci, I. Rusu, R. Chelariu, G. Bolat, C. Munteanu, D. Sutiman, R.M. Souto, Application of dynamic electrochemical impedance spectroscopy to the evaluation of the corrosion resistance of a historic bronze object in artificial acid rainwater, *European Journal of Science and Theology* 9 (2013) 189-199.
- [41] B. Yeum, *Electrochemical Impedance Spectroscopy: Data Analysis Software*, Echem Software, Ann Arbor, MI, 2001.
- [42] ISO 10993-2:2006, *Biological Evaluation of Medical Devices - Part 2: Animal Welfare Requirements*, International Organization for Standardization, Geneva, 2006.
- [43] L.C. Trincă, M. Fântânariu, C. Solcan, A.E. Trofin, L. Burtan, D.M. Acatrinei, S. Stanciu, B. Istrate, C. Munteanu, In vivo degradation behavior and biological activity of some new

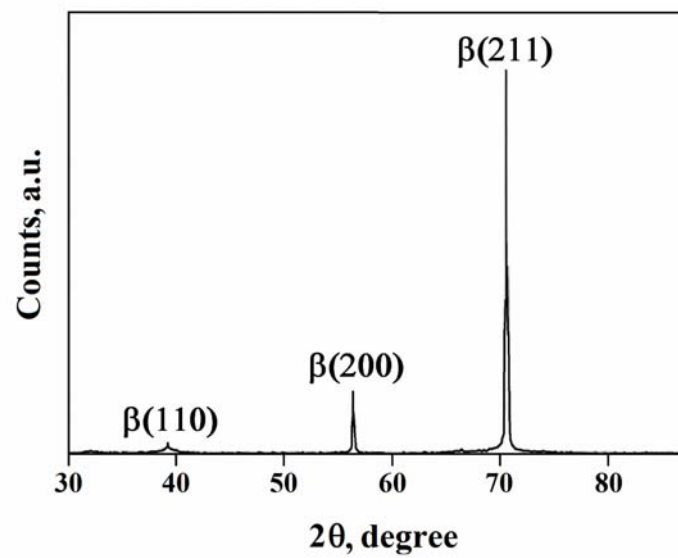
- Mg–Ca alloys with concentration's gradient of Si for bone grafts, *Applied Surface Science* 352 (2015) 140-150.
- [44] M. Fântânariu, L.C. Trincă, C. Solcan, A. Trofin, Ș. Strungaru, E.V. Șindilar, G. Plăvan, S. Stanciu, A new Fe-Mn-Si alloplastic biomaterial as bone grafting material: In vivo study, *Applied Surface Science* 352 (2015) 129-139.
- [45] M. Doube, M.M. Klosowski, I. Arganda-Carreras, F.P. Cordelières, R.P. Dougherty, J.S. Jackson, B. Schmid, J.R. Hutchinson, S.J. Shefelbine, BoneJ: Free and extensible bone image analysis in ImageJ, *Bone* 47 (2010) 1076-1079.
- [46] IBM Corp. Released 2012 IBM SPSS Statistics for Windows, Version 21.0., IBM Corp., Armonk, NY, 2012.
- [47] J.E.G. González, J.C. Mirza Rosca, Study of the corrosion behavior of titanium and some of its alloys for biomedical and dental implant applications, *Journal of Electroanalytical Chemistry* 471 (1999) 109-115.
- [48] J. Pan, H. Liao, C. Leygraf, D. Thierry, J. Li, Variation of oxide films on titanium induced by osteoblast-like cell culture, and influence of an H<sub>2</sub>O<sub>2</sub> pretreatment, *Journal of Biomedical Materials Research* 40 (1998) 244-256.
- [49] V.A. Alves, R.Q. Reis, I.C.B. Santos, D.G. Souza, T. de F. Gonçalves, M.A. Pereira-da-Silva, A. Rossi, L.A. da Silva, In situ impedance spectroscopy study of the electrochemical corrosion of Ti and Ti-6Al-4V in simulated body fluid at 25 °C and 37 °C, *Corrosion Science* 51 (2009) 2473-2482.
- [50] X. Cheng, S.G. Roscoe, Corrosion behavior of titanium in the presence of calcium phosphate and serum proteins, *Biomaterials* 26 (2005) 7350-7356.
- [51] S. Tamilselvi, N. Rajendran, Electrochemical studies on the stability and corrosion resistance of Ti-5Al-2Nb-1Ta alloy for biomedical applications, *Trends in Biomaterials & Artificial Organs* 20 (2006) 49-52.
- [52] S. Tamilselvi, R. Murugaraj, N. Rajendran, Electrochemical impedance spectroscopic studies of titanium and its alloys in saline medium, *Materials and Corrosion* 58 (2007) 113-120.
- [53] S. Tamilselvi, N. Rajendran, In vitro corrosion behaviour of Ti-5Al-2Nb-1Ta alloy in Hanks solution, *Materials and Corrosion* 58 (2007) 285-289.

- [54] S.E. Kim, J.H. Son, Y.T. Hyun, H.W. Jeong, Y.T. Lee, J.S. Song, J.H. Lee, Electrochemical corrosion of novel beta titanium alloys, *Metals and Materials International* 13 (2007) 151-154.
- [55] M.E.P. Souza, L. Lima, C.R.P. Lima, C.A.C. Zavaglia, C.M.A. Freire, Effects of pH on the electrochemical behavior of titanium alloys for implant applications, *Journal of Materials Science: Materials in Medicine* 20 (2009) 549-552.
- [56] B.L. Wang, Y.F. Zheng, L.C. Zhao, Effects of Hf content and immersion time on electrochemical behavior of biomedical Ti-22Nb-xHf alloys in 0.9% NaCl solution, *Materials and Corrosion* 60 (2009) 330-335.
- [57] C.W. Chan, H.C. Man, T.M. Yue, Effect of post-weld heat-treatment on the oxide film and corrosion behaviour of laser-welded shape memory NiTi wires, *Corrosion Science* 56 (2012) 158-167.
- [58] J.R. Macdonald, Note on the parameterization of the constant-phase admittance element, *Solid State Ionics* 13 (1984) 147-149.
- [59] T.P. Hoar, D.C. Mears, Corrosion-resistant alloys in chloride solutions materials for surgical implants, *Proceedings of the Royal Society A* 294 (1966) 486-511.
- [60] S. Khoshniat, A. Bourguine, M. Julien, P. Weiss, J. Guicheux, L. Beck, The emergence of phosphate as a specific signaling molecule in bone and other cell types in mammals, *Cellular and Molecular Life Sciences* 68 (2011) 205-218.
- [61] A. Muljačić, R. Poljak-Guberina, J. Turčić, O. Živković, M. Guberina, B. Klaić, The changes of bone-specific alkaline phosphatase (BsALP) associated with callus formation and rate of bone healing, *Croatica Chemica Acta* 83 (2010) 315-321.
- [62] M.O. Coulibaly, D.L. Sietsema, T.A. Burgers, J. Mason, B. Williams, C.B. Jones, Recent advances in the use of serological bone formation markers to monitor callus development and fracture healing, *Critical Reviews™ in Eukaryotic Gene Expression* 22 (2010) 629. doi:10.1016/j.bbi.2008.05.010.
- [63] U. Kini, B.N. Nandeesh, Physiology of bone formation, remodeling, and metabolism. In: *Radionuclide and Hybrid Bone Imaging*, Springer, Berlin, 2012, pp. 29-57.
- [64] Y. Okazaki, S. Rao, Y. Ito, T. Tateishi, Corrosion resistance, mechanical properties, corrosion fatigue strength and cytocompatibility of new Ti alloys without Al and V, *Biomaterials* 19 (1998) 1197-1215.

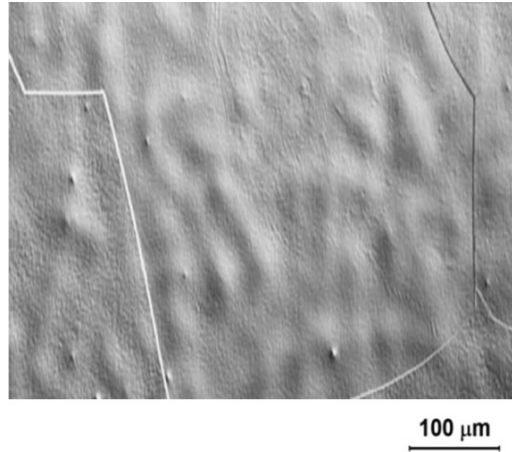
- [65] E. Delvat, D.M. Gordin, T. Gloriant, J.L. Duval, M.D. Nagel, Microstructure, mechanical properties and cytocompatibility of stable beta Ti-Mo-Ta sintered alloys, *Journal of the Mechanical Behavior of Biomedical Materials* 1 (2008) 345-351.
- [66] Q. Wang, Y. Qiao, M. Cheng, G. Jiang, G. He, Y. Chen, X. Zhang, X. Liu, Tantalum implanted entangled porous titanium promotes surface osseointegration and bone ingrowth, *Scientific Reports* 17 (2016) 26248, 13 pp. doi: 10.1038/srep26248.
- [67] J.L. Xu, S.C. Tao, L.Z. Bao, J.M. Luo, Y.F. Zheng, Effects of Mo contents on the microstructure, properties and cytocompatibility of the microwave sintered porous Ti-Mo alloys, *Materials Science and Engineering C* 97 (2019) 156-165.
- [68] M.L. Boussein, S.K. Boyd, B.A. Christiansen, R.E. Guldborg, K.J. Jepsen, R. Müller, Guidelines for assessment of bone microstructure in rodents using micro-computed tomography, *Journal of Bone and Mineral Research* 25 (2010) 1468-1486.



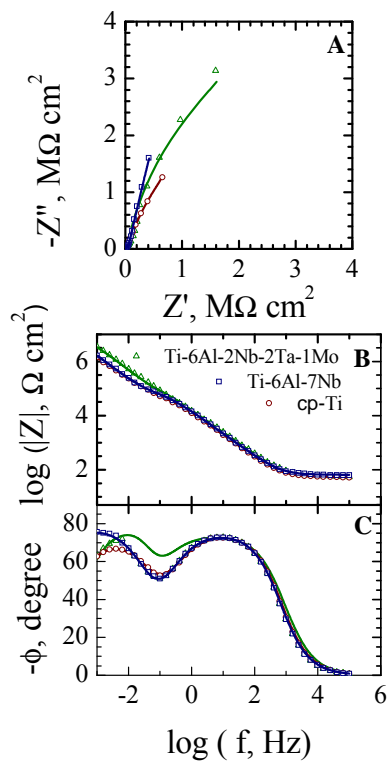
**Figure 1.** Main stages of the tibia implant surgery in the rabbit.



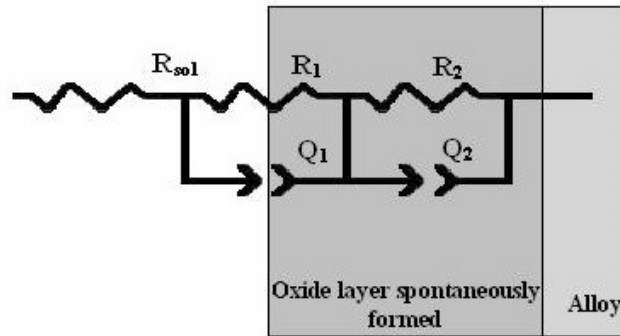
**Figure 2.** Representative X-ray diffractogram for  $\beta$  the metastable Ti-6Al-2Nb-2Ta-1Mo alloy.



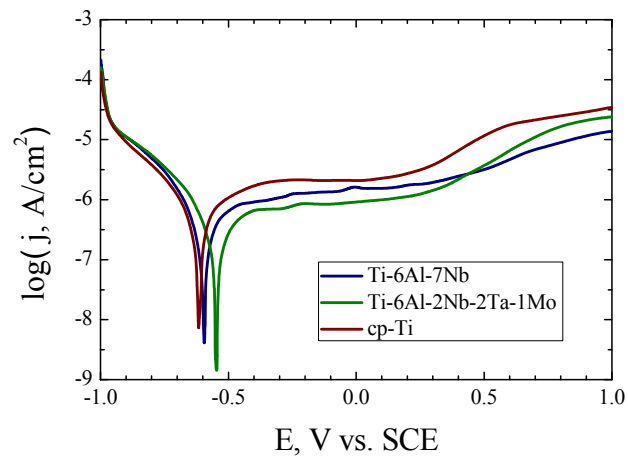
**Figure 3.** Optical micrograph of the Ti-6Al-2Nb-2Ta-1Mo alloy showing the grain microstructure.



**Figure 4.** Measured (discrete points) and fitted (solid lines) impedance spectra for Ti-6Al-2Nb-2Ta-1Mo alloy (by comparison with cp-Ti and Ti-6Al-7Nb samples) recorded at the corresponding open circuit potential during exposure to aerated HBSS at 37 °C. (A) Nyquist, and (B) Bode diagrams.

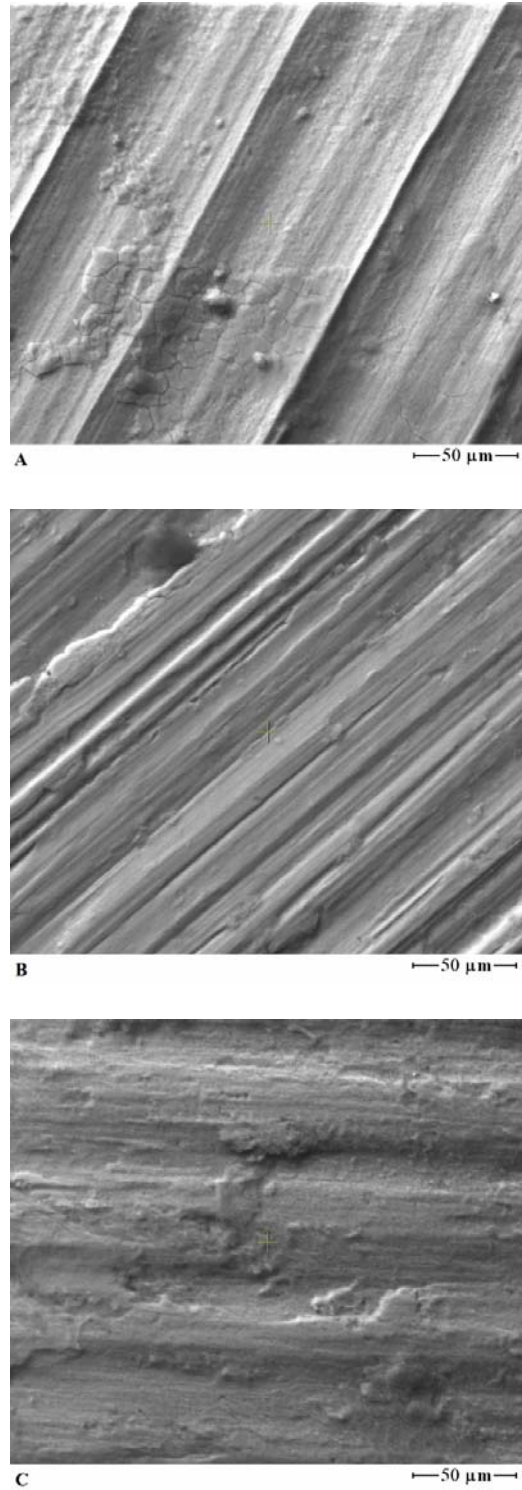


**Figure 5.** Equivalent circuit (EC) used in the generation of simulated data from the impedance spectra depicted in Figure 4.

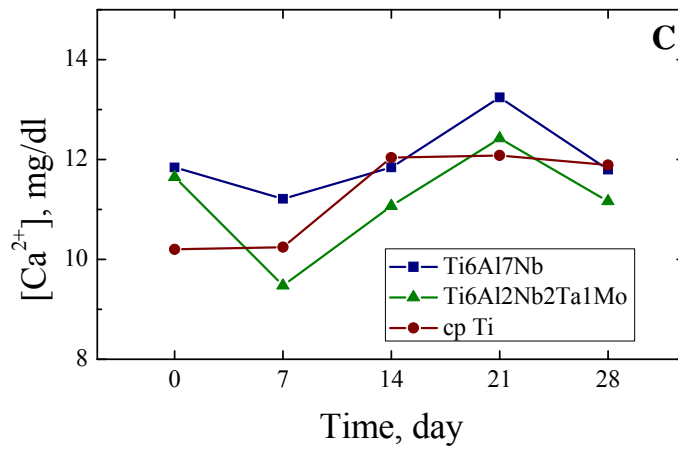
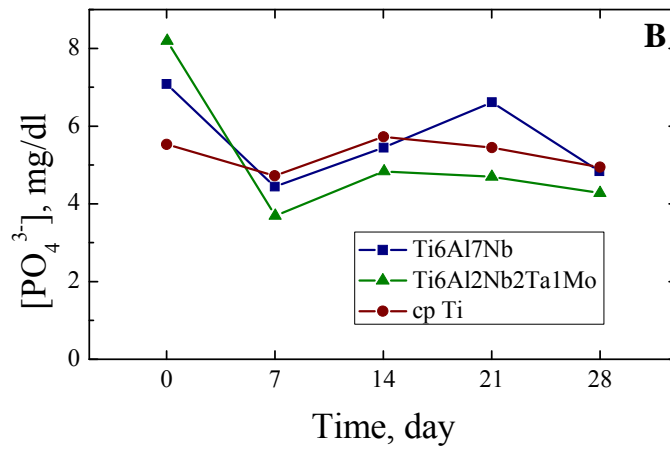
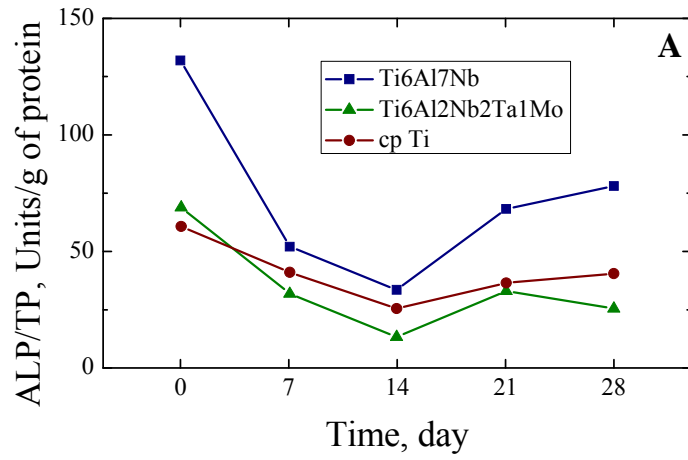


**Figure 6.** Linear potentiodynamic polarization curves of new Ti-6Al-2Nb-2Ta-1Mo alloy (by comparison with CpTi and Ti-6Al-7Nb samples) in aerated HBSS at 37 °C. Scan rate: 1 mV/s.

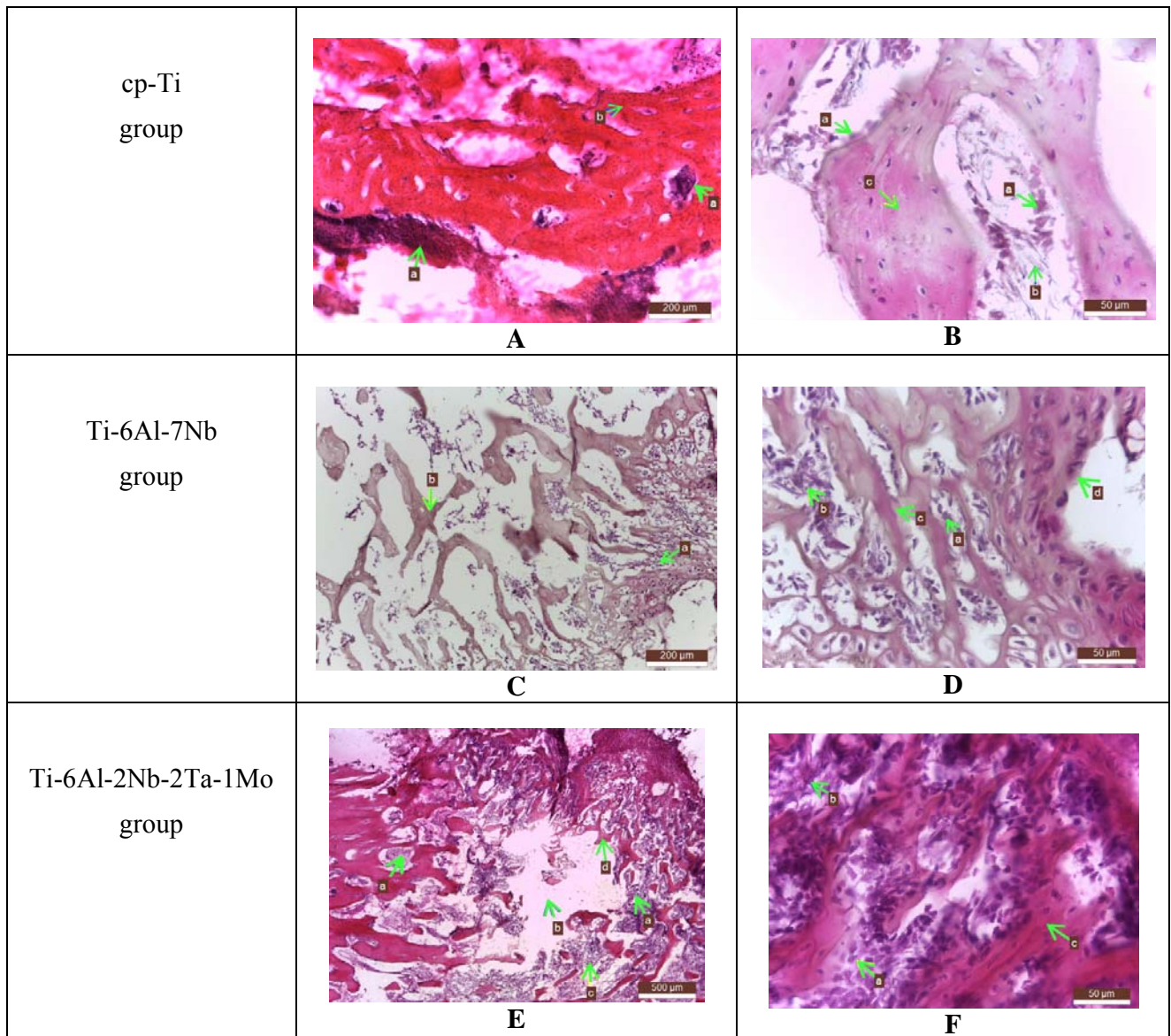




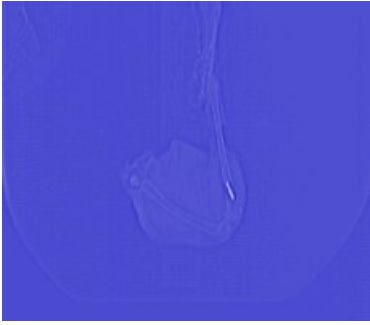


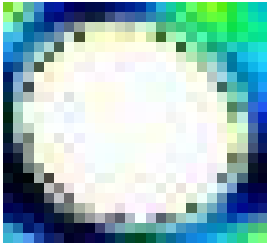
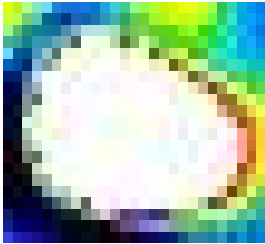
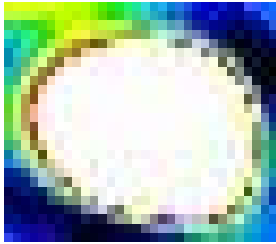
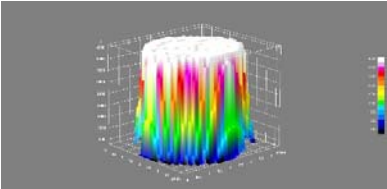
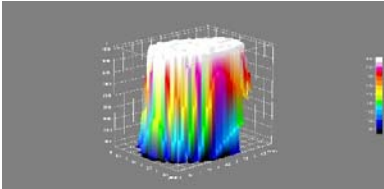
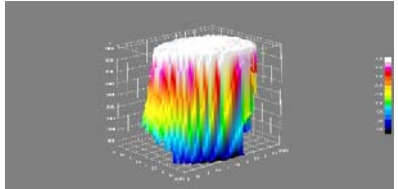
**Figure 7.** SEM images of corroded surfaces of: (A) cp-Ti, (B) Ti-6Al-7Nb, and (C) Ti-6Al-2Nb-2Ta-1Mo retrieved at +1.0 V<sub>SCE</sub> from HBSS after completing the potentiodynamic polarization tests.



**Figure 8.** Dynamics of blood serum mean values of total calcium, inorganic phosphate and alkaline phosphatase activity for the rabbit experimental model with tibial implant



**Figure 9.** Main histological features of the newly formed bone tissue coming from the rabbit experimental model with tibial implant

	cp-Ti	Ti-6Al-7Nb	Ti-6Al-2Nb-2Ta-1Mo
A			
B			
C			

**Figure 10.** Basic, 2D- and 3D- reconstructive CT images characterizing the integration of the implants in the osseous tissue. (A) Basic CT images showing the implanted material; (B) 2D-reconstructive images showing the degree of implant's surface coverage by the newly formed bone tissue; and (C) 3D-reconstructive images showing the spatial distribution of the newly formed bone tissue attached to the implant surface.

**Table 1.** Impedance parameters of the new Ti-6Al-2Nb-2Ta-1Mo alloy (by comparison with cp-Ti and Ti-6Al-7Nb samples) during exposure to aerated HBSS at 37 °C. The meaning of the impedance parameters corresponds to the equivalent circuit shown in Figure 5.

Sample	$Q_2,$ $s^n \mu S/cm^2$	$n_2$	$R_2,$ $k\Omega cm^2$	$Q_1,$ $s^n \mu S/cm^2$	$n_1$	$R_2,$ $M\Omega cm^2$
cp-Ti	15.9	0.84	74.6	28.3	0.81	7.90
Ti-6Al-7Nb	19.7	0.83	47.8	49.0	0.86	45.3
Ti-6Al-2Nb-2Ta-1Mo	13.5	0.83	239	10.8	0.95	113

**Table 2.** Corrosion parameters (and standard deviation values) determined from the potentiodynamic polarization curves measured for the new Ti-6Al-2Nb-2Ta-1Mo alloy (by comparison with cp-Ti and Ti-6Al-7Nb samples) in aerated HBSS at 37 °C.

Sample	ZCP, mV <sub>SCE</sub>	$\beta_a,$ mV/dec	$-\beta_c,$ mV/dec	$j_{cor}, \mu A/cm^2$
cp-Ti	-608 (11)	109 (8)	98 (5)	0.24 (0.03)
Ti-6Al-7Nb	-588 (11)	159 (9)	119 (7)	0.21 (0.03)
Ti-6Al-2Nb-2Ta-1Mo	-542 (9)	162 (9)	122 (7)	0.16 (0.02)

**Table 3.** Cortical bone morphometric indexes for the rabbit animal model with tibial implant.

Sample	BV, $mm^3$	TV, $mm^3$	BV/TV	Tb.Th Mean, mm	Tb.Th Std Dev, mm	Tb.Sp Mean, mm	Tb.Sp Std Dev, mm
cp-Ti	41.59	54.13	0.77	3.31	0.37	2.68	0.99
Ti-6Al-7Nb	20.29	25.35	0.80	2.86	0.16	2.34	0.74
Ti-6Al-2Nb-2Ta-1Mo	25.24	30.61	0.82	2.93	0.15	1.95	0.98